Flexible flapping wings can exhibit quasi-periodic motion!

Flexible flapping wings can exhibit quasi-periodic motion!

Chandan Bose[1] **& Sunetra Sarkar**[2]

[1] Department of Applied Mechanics, Indian Institute of Technology Madras, Chennai 600036, India

[2] Department of Aerospace Engineering, Indian Institute of Technology Madras, Chennai 600036, India

E-mail: cb.ju.1991@gmail.com, sunetra.sarkar@gmail.com

Abstract.

The dynamics of a flexible flapping wing is investigated by modelling it as a coupled nonlinear fluid-structure interaction (FSI) system in the low Reynolds number flow regime in accordance to the flight of flapping wing micro air vehicles (MAVs). A bifurcation analysis, by varying the free-stream wind velocity (U_∞) as the control parameter, revealed the presence of a new dynamics in the form of a quasi-periodic attractor in the flapping wing motion. The structural and aerodynamic nonlinearities present in the system cause a supercritical Hopf bifurcation, where stable limit cycle oscillation emerges from fixed point response beyond a critical value of the free-stream velocity. Further increasing the control parameter, another bifurcation named Neimark-Sacker bifurcation takes place and as a result, the flapping wing exhibits quasi-periodic motion. The presence of Neimark-Sacker bifurcation in the flapping flow-field dynamics is an interesting find and the present work focuses on it's associated dynamical behaviour. Various dynamical system tools like frequency spectra, phase space, Poincaré section, first return map have been implemented successfully to confirm the presence of quasi-periodicity.

1. Introduction

The amazing flying capability of insects has fascinated the researchers from the beginning of the twentieth century to investigate the unsteady aerodynamics of the flapping flight. The need for designing advanced flapping wing Micro Air Vehicles (MAVs) has boosted the research efforts in this direction. The combination of small dimensional size and slow speeds result in a low Reynolds number flight regime (10, 000 to 30, 000) which is well below the flight of conventional aircrafts. Hence at low Re, the viscous boundary layer is thicker and can result in a high drag and also there is deterioration of performance due to laminar boundary layer separation [1]. MAVs also experience highly unsteady flows in their environment and there is a need to overcome the additional drag and loss of lift without an increase in the size [2]. Thus, the natural flyers exploit the coupling between the unsteady flow and the wing deformation to enhance their aerodynamic performance in these adverse conditions.

With the change of kinematic, structural or aerodynamic parameters in a flapping flight, the wing-wake interaction can lead to an abrupt transition from periodicity to aperiodicity in the wake topology as well as in the aerodynamic loads which can indeed lead to an unpredictable body motion due to very low body inertia of extremely light weight flapping wing MAVs. This

underlines the need for specialized control algorithms. The aperiodic wake topology has been reported in recent literature in the flow past a rigid airfoil with forced flapping [3, 4, 5]. But unfortunately, there is no conclusive depiction of the transition from periodic to aperiodic regime from a dynamical systems point of view. Ashraf *et. al.* [5] has mentioned about the quasi-periodic transition to aperiodicity in the flow past a plunging airfoil based on the frequency spectra of the thrust coefficients. Although they have observed multiple peaks in the frequency spectra, no evidence in support of the existence of incommensurate frequencies was presented. Moreover, they have neglected the effect of flexibility and the subsequent fluid structure interaction effects, which is not realistic, especially when very light weight MAVs are involved.

As most of the earlier reported works discussing the dynamics of flapping wing MAVs such as Ashraf *et al.* [5] assumed the wing to be rigid, there is a crucial need to understand the role of structural flexibility on the overall dynamical performance. Further, most of the earlier works are either based on inviscid potential flows without considering any separations [6] or simplified point vortex models for leading edge vortices [7]. As such simplified models limit the understanding, we propose to use a full fidelity N-S solver in the present work. To summarize, the present work investigates the dynamics of flexible flapping systems in terms of the wing motion for comparable fluid-solid mass values (light weight MAVs) using a high fidelity flow solver.

The present FSI framework is comprised of a high fidelity Navier-Stokes based viscous aerodynamic solver and a structural model with cubic nonlinearity in the pitching motion, coupled by a weak coupling method. Bifurcation analysis considering Free stream velocity (U_∞) as the control parameter brings a new dynamics into light. It reveals that the flapping wing undergoes quasi-periodic motion in the presence of two incommensurate frequencies beyond a critical threshold of the control parameter. Nonlinear time series analysis has been carried out to categorize the dynamics.

This paper is organized as follows: Section 2 provides computational methodology, section 3 discusses the bifurcation analysis and the nonlinear time series analysis and finally this paper ends with the concluding remarks in section 4.

2. Computational methodology

2.1. Governing Equations and the Flow solver

The flow is governed by the incompressible Navier-Stokes (N-S) equation as follows,

$$\nabla.\vec{u} = 0, \ \frac{\partial \vec{u}}{\partial t} + [\vec{u}.\nabla]\vec{u} = -\nabla p/\rho + \nu\nabla^2\vec{u}. \tag{1}$$

Here, $\vec{u}$ is the velocity of the flow, p is the pressure, ν is the kinematic viscosity, ρ is the fluid density, $\nabla = \frac{\partial}{\partial x}\vec{i} + \frac{\partial}{\partial y}\vec{j}$, is the two dimensional gradient vector and t is time. The simulations are performed in OpenFOAM®, an open source finite-volume based CFD solver. The arbitrary Lagrangian Eulerian (ALE) formulation has been used for discretizing the N-S equation on a deformed flow mesh using radial basis function (RBF) interpolation scheme. The pressure-velocity coupling is achieved through PISO algorithm [9] with three PISO corrector loops. The algorithms used here for solving the pressure, velocity and mesh motion have been discussed in detail by Bos [10]. A rectangular computational domain shown in Fig.1 was used for the analysis. The computational domain is discretized using a combination of structured and unstructured grids as shown in Fig. 2. The grid independent study and the flow solver validation have been discussed in details in [11].

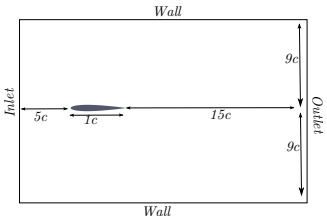

Figure 1. Computational domain

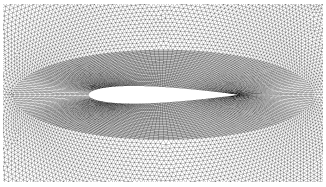

Figure 2. Close-up view of the mesh

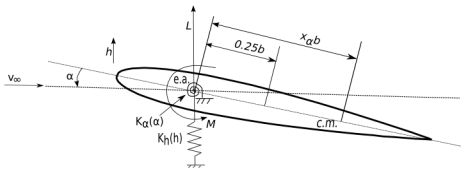

Figure 3. Schematic of a symmetric airfoil in pitch and plunge degrees of freedom

2.2. Structural solver

The structural part is comprised of an airfoil with pitch-plunge degrees of freedom as shown in Fig. 3. The airfoil is restrained by non-linear springs. The directions of positive lift and moment are indicated in the figure. The equations of motion are given by [6],

$$m\ddot{h} + S\ddot{\alpha} + C_h\dot{h} + K_h(h) = L(t),\ K_h(h) = K_{h1}h + K_{h2}h^3; \tag{2}$$

$$S\ddot{h} + I\ddot{\alpha} + C_\alpha\dot{h} + K_\alpha(\alpha) = M(t),\ K_\alpha(\alpha) = K_{\alpha1}\alpha + K_{\alpha2}\alpha^3. \tag{3}$$

In the above equations, h and α are the plunge and pitch displacements respectively, m is the mass of the airfoil, S is the first moment of inertia, I is the second moment of inertia, K_{h1}, K_{h2}, $K_{\alpha1}$ and $K_{\alpha2}$ are the spring stiffness coefficients, C_h and C_α are the damping coefficients, $L(t)$ is the unsteady lift and $M(t)$ is the moment about the quarter chord. Lift and moment are calculated by the flow solver at each time step. The structural response (Eq. 2-3) is solved using an explicit fourth-order Runge-Kutta method. The time step for integration is equal to that of the flow solver. A partitioned approach based weak coupling method has been used in the present investigation to couple the flow solver and the structural solver. In the partitioned approach, two separate solvers for fluid and structure are used jointly by exchanging information from one time step to another in an alternating fashion explicitly [12]. The coupling methodology has been discussed in details in [11].

3. Results and discussions

3.1. Bifurcation Analysis

Bifurcation analysis helps us to investigate the qualitative changes in the system behaviour by changing a control parameter. It is essential for the design of flexible flapping devices to define a stable operation regime. The flexible flapping wing studied here is inherently a coupled nonlinear dynamical system. In the present study, the flapping motion is limited to two degrees of freedom with pitch and plunge motion. The non-dimensionalised free-stream velocity ($U^* = \frac{U_\infty}{b\ \omega_\alpha}$) has been chosen as the bifurcation parameter to investigate its effect on the system dynamics. A schematic plot of the bifurcation diagram is presented in Fig. 4.

A summary of the dynamics of the FSI system in response to the change of the bifurcation parameter, U^* can be seen in Fig. 5. The value of the solid to fluid mass ratio is kept low at 5, in order to keep the focus on the light weight MAV wings. As we gradually increase the control parameter, a rich dynamics is revealed and multiple bifurcations take place with the dramatic qualitative change in the system behaviour. In order to investigate those changes, the pitch response is chosen to plot the bifurcation diagram. Corresponding to every U^*, the amplitudes of the local maxima in the computed time series of pitch response is plotted to get the upper branch of the bifurcation diagram. The number of local maxima, at a given parameter, gives the period of oscillations: a single local maximum indicates a limit cycle oscillation, two local maxima values suggest period two oscillations and so on.

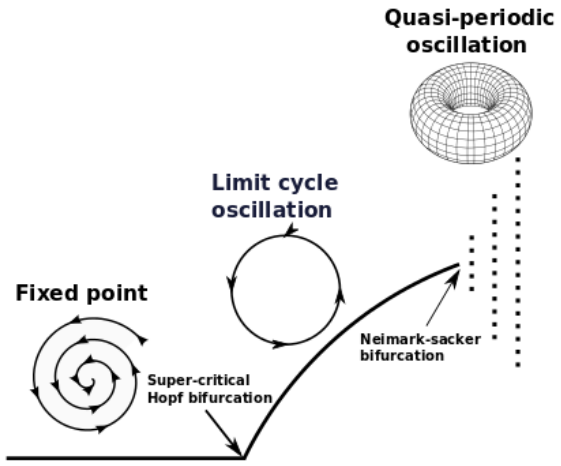

Figure 4. Schematic of the bifurcation diagram

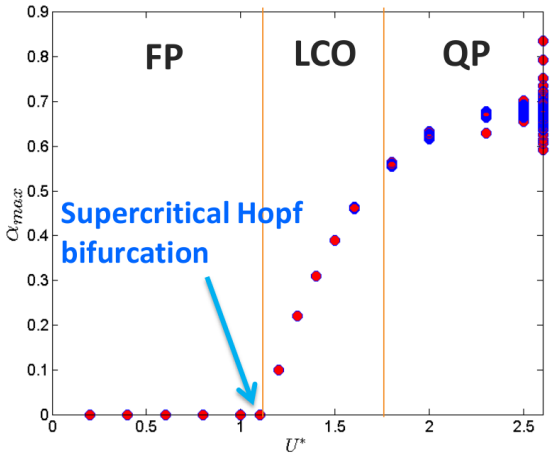

Figure 5. Bifurcation diagram of the FSI system

The first qualitative change takes place in the system at $U^* = 1.1$ where a supercritical Hopf-bifurcation takes place and as a result, a stable fixed point response becomes unstable and gives way to a stable self-excited limit cycle oscillation. The point at which the bifurcation occurs is called the "Hopf point". The amplitude of the single frequency LCO increases with the increase of bifurcation parameter. Further increasing the control parameter, beyond $U^* = 1.7$, another change in the dynamics is observed: a second Hopf bifurcation of the periodic solution occurs, introducing a new frequency which is incommensurate with the first one in the bifurcating solution. This kind of bifurcation is called a secondary Hopf or Neimark-Sacker bifurcation [13]. It occurs when two complex conjugate eigenvalues exit the unit circle away from the real axis. As a result, the system behaviour changes from limit cycle oscillation to quasi-periodic oscillation with two incommensurate frequencies. The local maxima in the oscillations no longer have a constant amplitude as additional frequencies appear in the response which are not harmonics of the earlier existing fundamental frequency. The regions of fixed point response, limit cycle oscillations and quasi-periodic oscillations are shown as the region of 'FP', 'LCO' and 'QP' respectively in Fig. 5.

3.2. Nonlinear time series analysis

For a better understanding of the dynamics and to confirm the type of bifurcations involved, nonlinear time series analysis tools such as time histories, state-space plots, Poincaré sections, first return maps and the frequency spectra are implemented in the present study. Nonlinear time series analysis techniques provide tools for systematic analysis and identification of specific signatures of time series data generated by a complex nonlinear system.

The time histories of the pitch response at different values of U^* are shown in Fig. 6 and the frequency spectra of the pitch response at $U^* = 2.6$ are presented in Fig. 7. The time history prior to the supercritical Hopf bifurcation shows a damped response where the response settles down to a stable equilibrium point beyond the transient motion. The time history of limit cycle oscillations has the appearance of a uniform trace as shown in Fig. 6(b) and the corresponding frequency spectra have one fundamental frequency in the form of a dominant peak. The envelope of time history for quasi-periodic response given in Fig. 6(c) looks different from that of Fig. 6(b) and shows uneven peaks. The corresponding frequency spectra of a two frequency quasi-periodic time history contain two fundamental peaks with an irrational

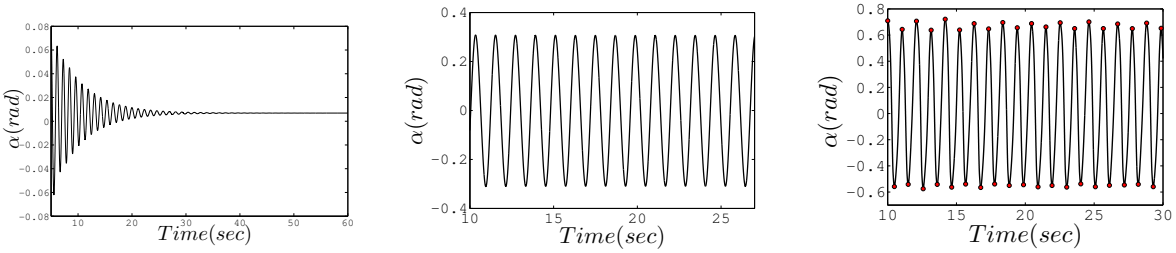

(a) $U^* = 1.0$ (b) $U^* = 1.3$ (c) $U^* = 2.6$

Figure 6. Time histories pitch response

frequency ratio attributing to two incommensurate frequencies. The other non-harmonic peaks occur as linear combinations of the two fundamental incommensurate frequencies. In case of $U^* = 2.6$, the frequency spectra clearly shows two incommensurate frequencies '$f1$' and '$f2$' and the other frequencies are '$f1+f2$', '$2f1+f2$', '$2f1$', '$3f1$', '$4f1$' and '$5f1$' which clearly indicate the linear combination of the mentioned incommensurate frequencies, $f1$ & $f2$ as shown in Fig. 7.

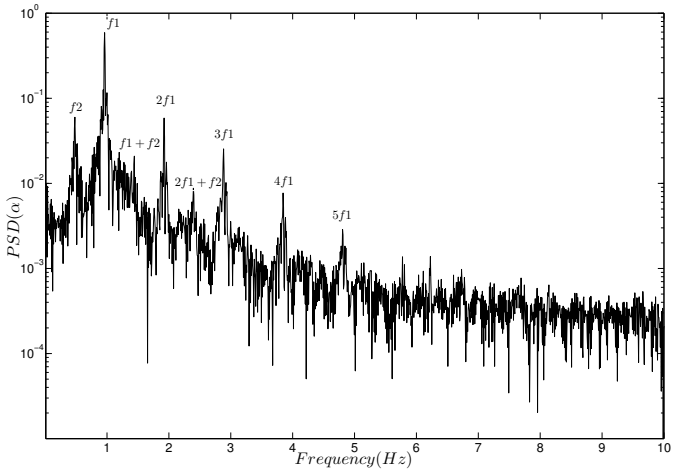

Figure 7. FFT of pitch response at $U^* = 2.6$

The space defined by the independent coordinates required to describe a motion is called a state space and the independent coordinates are called state variables [13]. In the present work, the physical state-space, projected in two dimensions, is constructed by the state variables (α, $\dot{\alpha}$). Phase space provides us a qualitative picture of the evolution of the trajectories and presence of the attractor of the system. The phase portraits for the pitch response at different U^* are presented in Fig. 8(a), 8(d) & 8(g). The phase portrait corresponding to the damped response of the wing is a stable spiral in the phase space as shown in Fig. 8(a), whereas the phase portrait of the limit cycle oscillation represents a unique closed one-dimensional attractor which depicts the periodic nature of the flapping motion as shown in Fig. 8(d). However, with the introduction of a new incommensurate frequency due to Neimark-Sacker bifurcation, the single loop turns into a dense toroidal structure. A toroidal structure in the phase space is an indication of quasi-periodic oscillations. Due to the presence of the incommensurate frequencies, the phase space trajectory evolves on the surface of a torus, never closing itself [14]. Among the three, the phase portrait corresponding to $U^* = 2.6$ is quasi-periodic and represents a shape of T^2 torus as shown in Fig. 8(g). The deformed shape of the attractor can be attributed to the fact that the quasi-periodic attractor is a superposition of two incommensurate fundamental frequencies and their harmonics [15].

A Poincaré section converts a continuous time evolution into a discrete time mapping. Thus, it is a very useful tool to characterize the time series whose phase space dimension is high (> 3). The reduced attractor is not identical to the original attractor but it preserves the topological properties of the original attractor [16]. In this present work, the Poincaré sections

have been constructed in a stroboscopic manner with the known time period of the limit cycle oscillation. Hence, the Poincaré section acts like a stroboscope, freezing the components of the motion commensurate with the limit cycle time period (say T). So, we will get a single point corresponding to the limit cycle oscillation, whereas if we get a collection of k (say) discrete points on the Poincaré section, the corresponding motion is periodic with the period kT. When the ratio of the added frequency and the limit cycle frequency is not a rational number, it denotes two frequency quasi-periodic motion and the points on the corresponding Poincaré section will fill up a closed smooth curve densely [13]. The Poincaré sections for the pitch response have been plotted for $U^* = 1, 1.3, 2.6$ in Fig. 8(b), 8(e) & 8(h) respectively. As discussed above, they correspond to the damped, periodic and quasi-periodic dynamics.

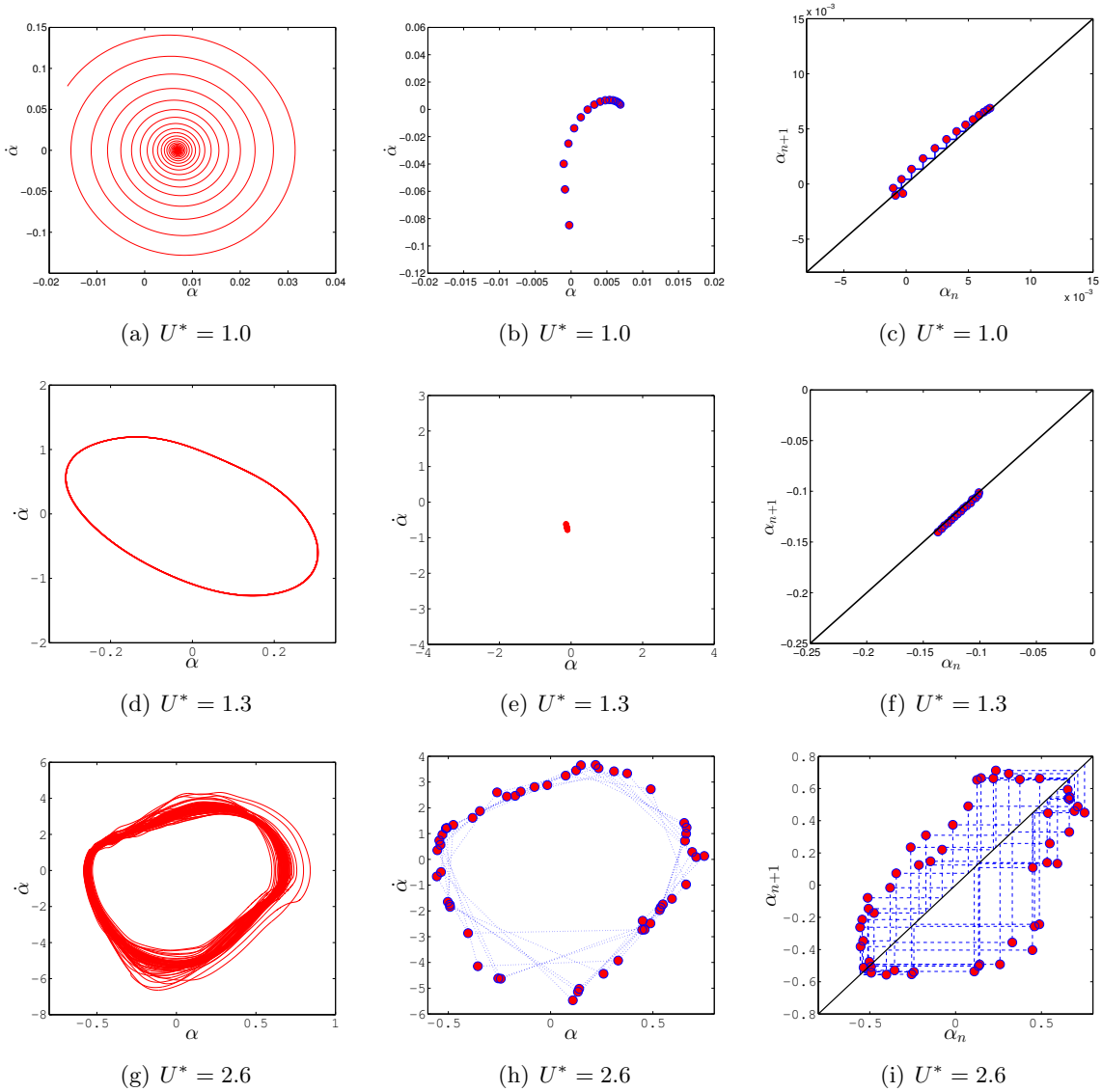

(a) $U^* = 1.0$ (b) $U^* = 1.0$ (c) $U^* = 1.0$

(d) $U^* = 1.3$ (e) $U^* = 1.3$ (f) $U^* = 1.3$

(g) $U^* = 2.6$ (h) $U^* = 2.6$ (i) $U^* = 2.6$

Figure 8. Phase portraits (left), Poincaré sections (middle) & first return maps (right)

To analyze the dynamics further, we have implemented 1D mapping technique of first return map which is essentially constructed from the Poincaré sections as discussed before. Using the first return map, we investigate the evolution of the discretized version of the system derived

from the continuous evolution. In the first return map, the points on the phase space frozen by the stroboscopic Poincaré section (x_n) are collected and they are plotted against the next iterates (x_{n+1}) that occur and a 2D plot (x_n) vs (x_{n+1}) is obtained. For a periodic attractor, the successive iterates are equal, hence mapping lies on the $x = y$ diagonal, else it moves away from the diagonal. Thus, a first return map can be utilized to explore the evolution of the phase space trajectories in a lower dimensional space preserving the same properties. Fig. 8(c), Fig. 8(f) & Fig. 8(i) present first return maps for damped response, limit cycle oscillation and quasi-periodic attractor respectively. The first return map for a limit cycle oscillation is represented by a diagonal line along $x = y$ line, whereas it is a loop in the case of a quasi-periodic state. Further, the cobweb diagrams are constructed to understand the evolution of the iterates of the return map.

4. Conclusion

A new dynamics of quasi-periodicity is observed in the motion of a flexible flapping wing in the bifurcation analysis considering the non-dimensional free-stream velocity as the control parameter. It has been observed that with the increase of the control parameter, at first, a supercritical Hopf bifurcation takes place at a critical value of the parameter due to which the flapping motion undergoes a self-sustained LCO. Thereafter, further increasing the control parameter, a Neimark-Sacker bifurcation occurs over the LCO making the flapping motion quasi-periodic. The time series of pitch response has been categorized using nonlinear time series analysis tools. The existence of the incommensurate frequencies in the frequency spectra of the pitch response at $U^* = 2.6$ is evidently shown in the present study. Further, the toroidal phase space along with the closed Poincaré section and a loop structure in the first return map confirm the quasi-periodic nature of the pitch response at $U^* = 2.6$. For the future work, the authors are working to understand the dynamics of the flapping wing at the higher control parameter values beyond quasi-periodic dynamics.

References

[1] Mueller T J & DeLaurier J D 2003 *Annual Review of Fluid Mechanics* **35(1)** 89-111
[2] Young J 2005 *Ph.D. Thesis, University of New South Wales, Australian Defence Force Academy, School of Aerospace, Civil and Mechanical Engineering.*
[3] Blondeaux P, Guglielmini L & Triantafyllou M S 2005 *AIAA Journal* **43** 918-922
[4] Lentink D, Heijst G F V, Muijres F T & Leeuwen J L V 2010 *Biology Letters, rsbl20090806*
[5] Ashraf M A, Young J & Lai J C S 2012 *AIAA Journal* **50(11)** 23082324
[6] Lee B H K, Jiang L Y & Wong Y S 1999 *Journal of Fluids and Structures* **13 (1)** 75-101
[7] Ramesh K, Murua J & Gopalarathnam A 2015 *Journal of Fluids and Structures.* **55** 84-105
[8] Bos F M, Van Oudheusden B W, & Bijl H 2013 *Computers and Fluids* **79** 167-177.
[9] Ferziger J & Peric M 2002 *Computational Methods for Fluid Dynamics,3rd edition, Springer-Verlag, Berlin.*
[10] Bos F M, Van Oudheusden B W, & Bijl H 2013 *Journal of Fluids and Structures* **42** 130-151.
[11] Bose C, Badrinath S, Gupta S, & Sarkar S 2016 *Procedia Engineering* **144** 883-890.
[12] Michler C, Hulshoff S, Van Brummelen E & De Borst R 2004 *Computers & fluids* **33** 839-348.
[13] Nayfeh A H, & Balachandran B 2008 *Applied Nonlinear Dynamics: Analytical, Computational and Experimental Methods. John Wiley & Sons.*
[14] Kabiraj L, Saurabh A, Wahi P, & Sujith R I 2012 *Chaos: An Interdisciplinary Journal of Nonlinear Science* **22(2)** 023129
[15] Saha A K, Muralidhar K & Biswas G 2000 *Journal of Engineering Mechanics* **126(5)** 523-532
[16] Berge P, Pomeau Y, & Vidal C 1984 *Order within Chaos. Wiley and Sons.*